ARTICLES
PUBLISHED ONLINE: 24 NOVEMBER 2013 | DOI: 10.1038/NPHYS2805
nature physics

Inelastic X-ray scattering in $YBa_2Cu_3O_{6.6}$ reveals giant phonon anomalies and elastic central peak due to charge-density-wave formation

M. Le Tacon[1]*, A. Bosak[2], S. M. Souliou[1], G. Dellea[3], T. Loew[1], R. Heid[4], K-P. Bohnen[4], G. Ghiringhelli[3], M. Krisch[2] and B. Keimer[1]*

The electron–phonon interaction is a major factor influencing the competition between collective instabilities in correlated-electron materials, but its role in driving high-temperature superconductivity in the cuprates remains poorly understood. We have used high-resolution inelastic X-ray scattering to monitor low-energy phonons in $YBa_2Cu_3O_{6.6}$ (superconducting transition temperature $T_c = 61$ K), which is close to a charge-density-wave (CDW) instability. Phonons in a narrow range of momentum space around the CDW ordering vector exhibit extremely large superconductivity-induced line-shape renormalizations. These results imply that the electron–phonon interaction has sufficient strength to generate various anomalies in electronic spectra, but does not contribute significantly to Cooper pairing. In addition, a quasi-elastic 'central peak' due to CDW nanodomains is observed in a wide temperature range above and below T_c, suggesting that the gradual onset of a spatially inhomogeneous CDW domain state with decreasing temperature is a generic feature of the underdoped cuprates.

The character of the electron–phonon interaction (EPI) in metals and superconductors with strongly correlated electrons has recently been the subject of intense research, especially with regard to its influence on high-temperature superconductivity in the copper oxides[1–3]. Whereas density-functional theory (DFT) predicts only weak EPIs in these materials[4–7], various anomalies in the dispersion relations of both conduction electrons and lattice vibrations have been interpreted as evidence of an EPI strength far exceeding these predictions. In particular, the energies of prominent 'kinks' in the electronic band dispersions[8–11] were reported to be in good agreement with those of Cu–O bond vibrations that also exhibit sizable dispersion anomalies[12–14]. However, it has proved difficult to disentangle the influence of the EPI on these anomalies from other factors including spin fluctuations and lattice anharmonicity, respectively. The question of whether strong correlations substantially modify the EPI in the cuprates with respect to standard DFT therefore remains open, as do more general questions about the role of the EPI in driving high-temperature superconductivity and/or competing instabilities such as 'stripe' or CDW order. Similar questions are being asked for other correlated metals including the recently discovered iron-based superconductors.

We approached these issues from a new direction, following leads from recent X-ray scattering experiments that revealed strong CDW correlations in underdoped $YBa_2Cu_3O_{6+x}$, one of the most widely studied high-temperature superconductors[15–19]. Specifically, the CDW was shown to be present throughout the bulk of the material, clearly separated from magnetically ordered states, and competing strongly with superconductivity. $YBa_2Cu_3O_{6+x}$ is therefore well suited as a platform for the investigation of the role of the EPI as a mediator of collective ordering phenomena in the cuprates. However, the X-ray experiments reported thus far were carried out either in energy-integrating mode, or with an energy resolution insufficient to discriminate static and dynamic CDW correlations. Individual phonon modes could not be resolved in any of these experiments.

With this motivation, we have used non-resonant inelastic X-ray scattering (IXS) with high energy resolution to carefully monitor the temperature dependence of low-energy lattice vibrations around the CDW ordering wavevector of underdoped $YBa_2Cu_3O_{6.6}$. We observed pronounced phonon anomalies at energies that correspond well to those of recently discovered low-energy 'kinks' in the electronic bands of cuprates at similar doping levels[10,11]. These anomalies confirm a large EPI that is, however, highly anisotropic and confined to a very narrow window of momentum space. In addition, we discovered a quasielastic 'central peak' whose intensity is maximal at T_c, but persists over a wide temperature range above T_c. In analogy to classical work on structural phase transitions[20,21], we interpret this observation as evidence of a spatially inhomogeneous state in which lattice defects nucleate CDW nanodomains.

The IXS experiments were performed on an underdoped $YBa_2Cu_3O_{6.6}$ single crystal with $T_c = 61$ K previously studied with soft X-rays[15,19]. In such experiments, the phonon intensity depends on the total momentum transfer $\mathbf{Q}$, rather than the reduced momentum $\mathbf{q} = \mathbf{Q} - \mathbf{G}_{HKL}$, where $\mathbf{G}_{HKL}$ stands for the Brillouin zone centre, Γ, closest to $\mathbf{Q}$. As high-resolution IXS measurements are performed with high-energy (~20 keV) photons, the Ewald

[1]Max-Planck-Institut für Festkörperforschung, Heisenbergstraße 1, D-70569 Stuttgart, Germany, [2]European Synchrotron Radiation Facility, BP 220, F-38043 Grenoble Cedex, France, [3]CNR-SPIN, CNISM and Dipartimento di Fisica, Politecnico di Milano, Piazza Leonardo da Vinci 32, I-20133 Milano, Italy, [4]Institut für Festkörperphysik, Karlsruher Institut für Technologie (KIT), PO Box 3640, D-76021 Karlsruhe, Germany. *e-mail: m.letacon@fkf.mpg.de; b.keimer@fkf.mpg.de

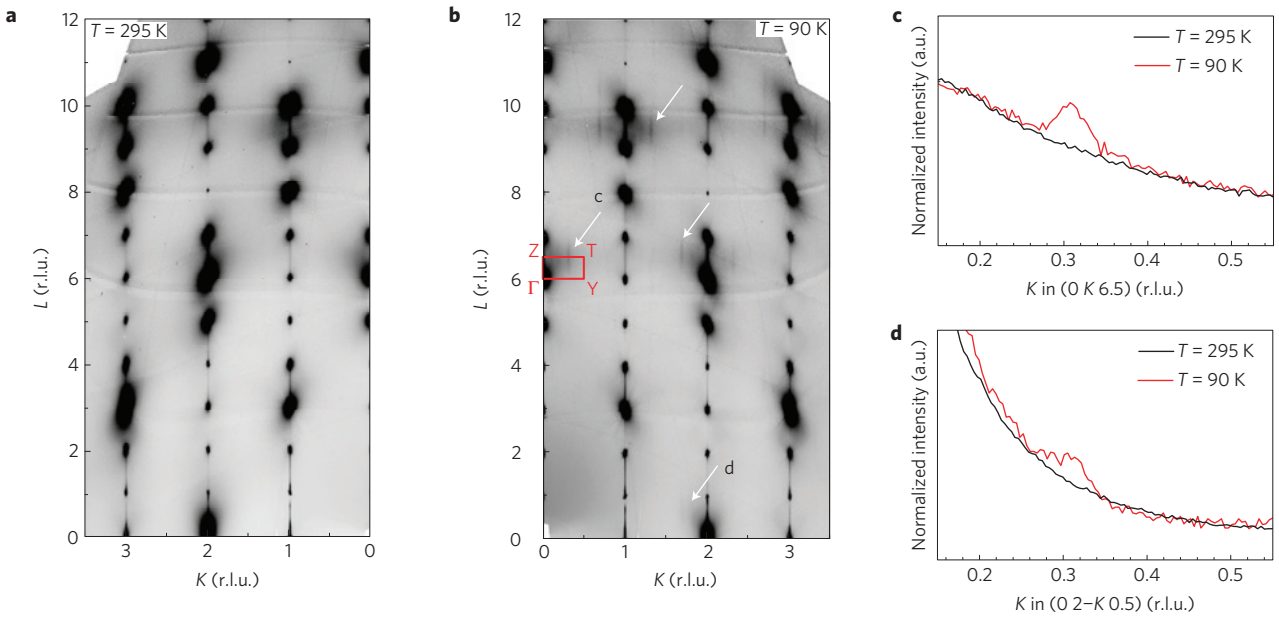

Figure 1 | Diffuse scattering mapping. a,**b**, Diffuse scattering mapping of the $\mathbf{Q} = (0\,K\,L)$ plane at room temperature (**a**) and at $T = 90$ K (**b**). K and L are given in reciprocal lattice units (r. l. u.). White arrows indicate the CDW superstructure peaks. **c**,**d**, Display cuts of these maps along (0 K 6.5) and (0 2–K 6.5), respectively. The red rectangle corners correspond to the Γ, Y, T and Z points of the Brillouin zone centred at $\mathbf{Q} = (0\,0\,6)$.

sphere encompasses hundreds of Brillouin zones. Before the IXS experiments, we therefore assembled a comprehensive map of the diffuse scattering intensity to identify the Brillouin zones with the most intense X-ray signatures of CDW formation. This method has recently been applied successfully to the study of low-energy phonons in other compounds including 2H-NbS_2 (ref. 22) and $ZrTe_3$ (ref. 23). In $YBa_2Cu_3O_{6.6}$, a short-range superstructure of oxygen dopants ('ortho-VIII structure')[24,25] gives rise to intense diffuse features in the $(H\,0\,L)$ plane of reciprocal space (Supplementary Information), which obscure the CDW reflections. We therefore focused on the $(0\,K\,L)$ plane, where the intensity maps (Fig. 1a,b) reveal the emergence of extended features at low temperatures. The positions, $\mathbf{q}_{CDW} = (0\,0.31\,0.5)$, and correlation lengths of these features (Fig. 1c,d) are compatible with those of the CDW reflections reported previously on the same material[15,16]. Their structure factor depends strongly on both K and L, mirroring the complex ionic displacement pattern associated with CDW formation. In the following, we will focus on transverse acoustic and optical phonons in the Brillouin zone adjacent to $\mathbf{G}_{006}$, where the CDW features are particularly intense. Similar results were obtained for longitudinal phonons near $\mathbf{G}_{020}$ (Supplementary Information).

Figure 2 shows a survey of the phonon dispersions and IXS intensity in this Brillouin zone at room temperature, along with the results of DFT calculations in several high-symmetry directions of momentum space[5]. The agreement between the experimental results and the DFT data is very reasonable, considering that the calculations were performed for fully oxygenated $YBa_2Cu_3O_7$. The low-energy IXS intensity is well described by DFT and is dominated by two modes. These correspond to a transverse acoustic and a transverse optical phonon, which belong to the B_1 representation along line Z–T marked in Figs 1 and 2 (Supplementary Information), and that mostly involve atomic vibrations along the c axis. The constant-$\mathbf{q}$ profiles discussed below therefore exhibit a two-peak structure.

The temperature evolution of the phonon profiles in the vicinity of $\mathbf{q}_{CDW}$ is shown in Fig. 3. The full IXS spectrum (Fig. 2b–g and Supplementary Information) is composed of Stokes and anti-Stokes components due to phonon creation and annihilation. As expected on the basis of the detailed-balance theorem, the ratio between Stokes and anti-Stokes intensities everywhere in momentum space was observed to be perfectly described by the Bose thermal excitation factor (Supplementary Information). We note that this is in contrast to a recent report of deviations from detailed balance in a different cuprate[26]. The temperature-dependent spectra of Fig. 3d–f were therefore normalized by dividing out the Bose factor. The spectra were fitted to standard damped harmonic oscillator profiles convoluted with the experimental resolution function whose energy and in-plane momentum resolution were set to 3 meV and 0.015 reciprocal lattice units (full-width at half-maximum, FWHM), respectively. Figure 4 shows the results of these fits. Whereas the phonon dispersions at $T = 150$ K are identical to those at room temperature (Fig. 2) within the experimental error, and phonon linewidths are limited by the instrumental energy resolution, marked anomalies are observed at lower temperatures.

We first focus on the behaviour in the superconducting state, where the dispersions of both phonons exhibit pronounced dips in the vicinity of $\mathbf{q} = \mathbf{q}_{CDW}$ (Figs 3a and 4a,b). These anomalies are not visible in the results of the DFT calculation, and, as they are restricted to a very narrow $\mathbf{q}$-range around $\mathbf{q}_{CDW}$, they were apparently not recognized in previous experimental work on the lattice dynamics of $YBa_2Cu_3O_{6+x}$. Some aspects of these dispersion anomalies are reminiscent of anomalous phonon softening and broadening effects that have been reported for higher-energy Cu–O bond-bending and bond-stretching phonons at comparable wavevectors[12,13]. As the anomalies reported here involve some of the lowest energy phonons, their contribution to electron–phonon coupling should be significantly higher.

Similar soft phonon modes have been observed in other compounds with quasi-one-dimensional[23,27] (quasi-1D) and quasi-2D (refs 22,28) electronic structure that either exhibit CDW order[23,27,28], or are on the verge of a CDW transition[22]. Remarkably, the sharpness of the dispersion anomaly in $YBa_2Cu_3O_{6.6}$ closely resembles those associated with 'Kohn anomalies' in quasi-1D CDW compounds with strongly nested Fermi surfaces[23,27]. In contrast, the phonon anomalies associated with quasi-2D CDWs are considerably broader[22,28], reflecting the less pronounced nesting of the associated Fermi surfaces. Model calculations for cuprates

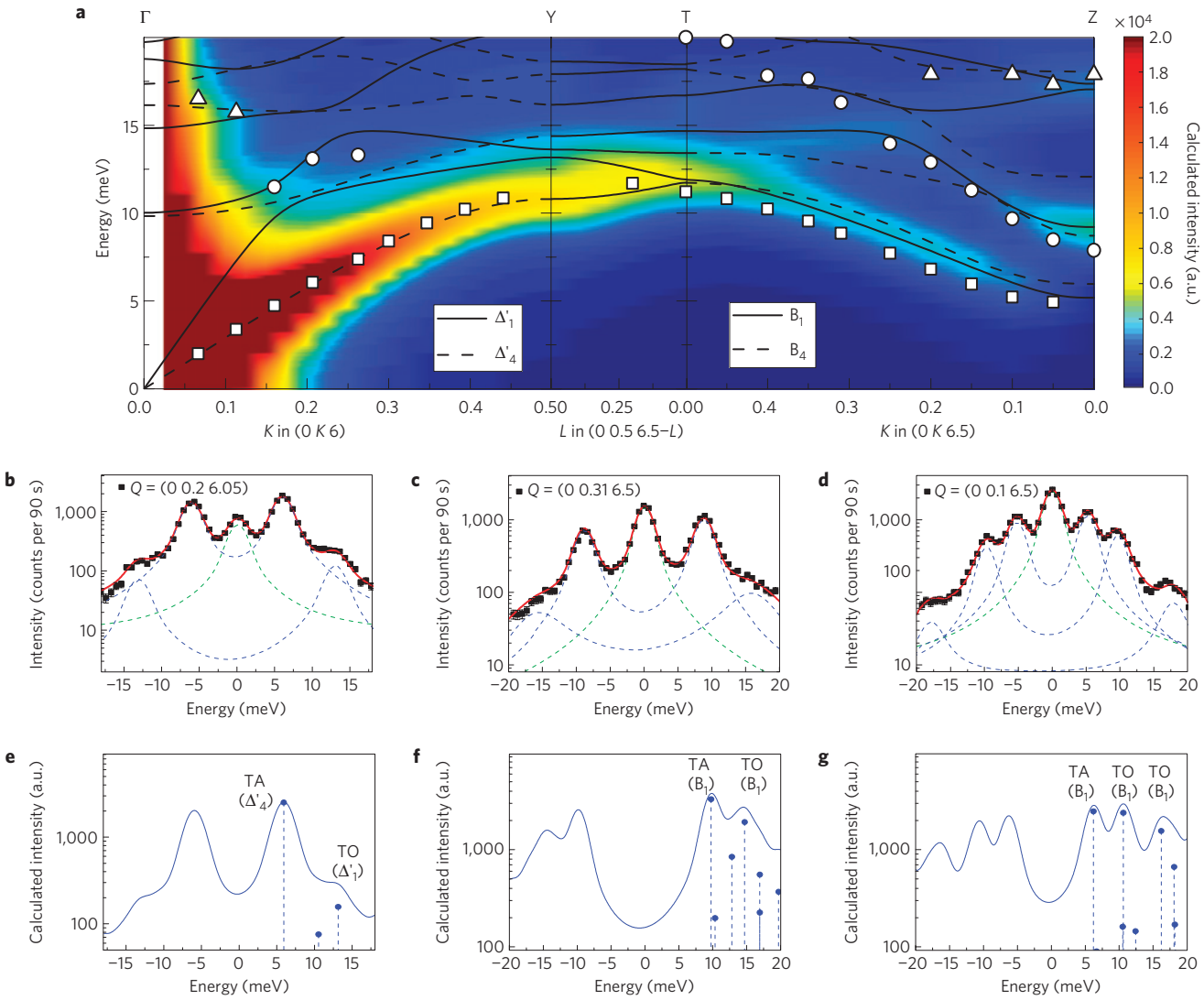

Figure 2 | Room-temperature phonon dispersions along the high-symmetry lines Γ–Y, Y–T and T–Z. a, The white symbols represent the results of an analysis of IXS profiles, as described in the text. The lines and colour map represent the results of DFT calculations for the phonon dispersions and IXS intensities calculated close to Γ = (0 0 6), respectively (Supplementary Information). These scattering geometries primarily select transverse acoustic (TA) and transverse optic (TO) branches in irreducible representations Δ_1' and Δ_4' along the Γ–Y, and B_1 along the Z–T direction. **b**–**d**, The IXS data taken at room temperature at reciprocal space points (0 0.2 6.05), (0 0.31 6.5) and (0 0.1 6.5). The statistical error bars are approximately equal to the size of the dots. The dashed green (blue) lines represent the results of fits to the elastic (inelastic) intensity, and the red line is the sum of these contributions. **e**–**g**, Plots of the calculated phonon intensity at these three points. The blue dots represent the contributions of individual phonons.

(which also exhibit quasi-2D Fermi surfaces) in the vicinity of CDW transitions yield Kohn anomalies whose widths are comparable to those of other quasi-2D CDW compounds, but much broader than those observed experimentally[29]. However, previous scanning tunnelling spectroscopy (STS) experiments have shown that the low-energy electronic transitions in the superconducting state of Bi-based cuprates are dominated by a small set of sharply defined wavevectors, as a consequence of the nesting properties of the *d*-wave gap function[30–34]. A detailed analysis of IXS and STS data on the same material is required to quantitatively assess the correspondence between the Kohn anomalies shown in Fig. 4a and the 'quasiparticle interference patterns' observed by STS. The same applies to recent photoemission data[10,11] on low-energy 'kinks' in the band dispersions of $Bi_2Sr_2CaCu_2O_{8+\delta}$, whose energies are in good agreement with those of our Kohn anomalies. We also note that the recovery signals in recent pump–probe experiments on underdoped $YBa_2Cu_3O_{6+x}$ (ref. 35) and $La_{1.9}Sr_{0.1}CuO_4$ (ref. 36) exhibit oscillations with frequencies that closely agree with those of the anomalous acoustic phonons we have observed.

We now turn to the behaviour at higher temperatures, which is even more surprising. On heating up to T_c, the phonon energy is weakly T-dependent (although a slight softening of the acoustic phonon at $\mathbf{q} = \mathbf{q}_{CDW}$ is noticeable, Fig. 4b), and the linewidth remains resolution-limited over the entire Brillouin zone, presumably because the maximum of the superconducting gap exceeds the phonon energy. At T_c, however, the frequency of the transverse acoustic phonon at $\mathbf{q}_{CDW}$ abruptly jumps by about 15% to its normal-state value; the hardening of the optical mode even exceeds 20%. At the same time, the phonon linewidths become extremely large in a narrow range around $\mathbf{q} = \mathbf{q}_{CDW}$, where the FWHM of the transverse acoustic phonon at T_c amounts to 3.5 meV, ~40% of its energy. On further heating, the phonon frequency is approximately T-independent, although the mode gradually narrows. The linewidth becomes resolution-limited

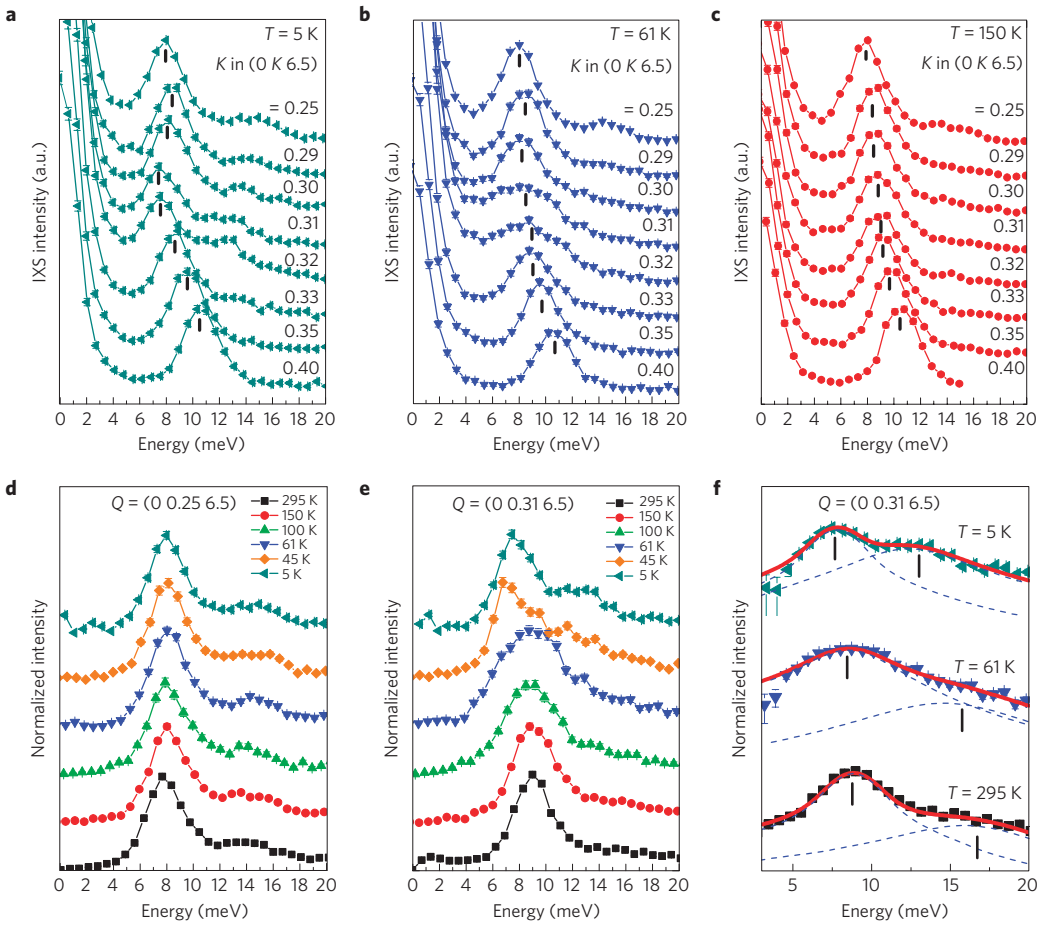

Figure 3 | Temperature dependence of the phonon spectra. a–c, Momentum dependence of the IXS spectra along the Z–T direction of reciprocal space at $T = 5$ K (**a**), $T = T_c = 61$ K (**b**) and $T = 150$ K (**c**). The error bars indicate the statistical error (s.d. to the number of detected photons). Black tick marks represent the phonon energy as extracted from fits to damped harmonic oscillator profiles (Supplementary Information). **d**,**e**, The temperature dependence of the inelastic part of the IXS spectra at $\mathbf{q} = (0\ 0.25\ 6.5)$ (**d**) and $\mathbf{q} = \mathbf{q}_{CDW} = (0\ 0.31\ 6.5)$ (**e**). The intensities shown in these two panels were corrected for the Bose excitation factor, and then normalized to the intensity of the low-energy peak. **f**, Details of the fits of the IXS spectra at $\mathbf{q}_{CDW}$ at 5, 61 and 295 K. A logarithmic scale has been used for the *y* axis for clarity. The dashed lines and tick marks indicate the individual phonon profiles resulting from the fits and their maxima, respectively.

around $T \sim 150$ K, where we observed the onset of the CDW peak in the same sample using resonant X-ray scattering[15].

On a qualitative level, the superconductivity-induced phonon anomaly we observed is in line with the generic behaviour of low-energy phonons in superconductors, which are expected to broaden and harden when the energy gap collapses and low-energy electron–phonon decay channels open up on heating above T_c. This behaviour has indeed been confirmed both for acoustic phonons in conventional superconductors[21,37] and for $\mathbf{q} = 0$ optical modes in $YBa_2Cu_3O_7$ and other cuprates[38,39], but these effects do not exceed a few per cent. We cannot completely rule out that the observed effect on the optical mode involves subtleties such as spectral weight transfer and/or anti-crossing with a neighbouring phonon (with at least twice lower intensity according to DFT calculation; see Supplementary Information). In any case, the magnitude of the superconductivity-induced phonon anomalies reported here is by far the largest reported in cuprates, undoubtedly as a consequence of the close competition between superconducting and CDW ground states in this material. To further elucidate the nature of this competition, we now take a detailed look at the IXS data above T_c (Fig. 5). The spectra are composed of an inelastic component due to Stokes and anti-Stokes scattering from phonons, as discussed above, and an elastic component centred at zero energy. The elastic line is T-independent and smoothly $\mathbf{Q}$-dependent over most of the Brillouin zone (Fig. 5a), and can thus be attributed to incoherent scattering from defects. For $\mathbf{q} = \mathbf{q}_{CDW}$, however, we observe an additional contribution to the elastic intensity (Fig. 5b,c). The T-dependent intensity and $\mathbf{q}$-width of this contribution are in excellent agreement with those inferred from the quasi-elastic scattering previously determined by resonant X-ray scattering experiments either without energy discrimination (inset in Fig. 5c) or with a much poorer resolution of ~100 meV (ref. 15). In our high-resolution experiments, the CDW component of the elastic line remained energy-resolution-limited even after we enhance the energy resolution to ~1.4 meV FWHM (Supplementary Information). Detailed analysis of the elastic peak and of the Stokes and anti-Stokes part of spectra allows us to put an upper bound of ~100 μeV on the intrinsic energy width of the elastic component of the CDW signal. This implies that CDW domains with characteristic fluctuation energies below ~100 μeV and typical dimensions of 1–10 nm (inferred from the momentum widths of the CDW peaks) are present in a wide temperature range both above and below T_c. As this upper bound is still far above the characteristic energy scale of nuclear magnetic resonance (NMR) and nuclear quadrupole resonance, slow fluctuations of the CDW domains may preclude their observation by nuclear resonance techniques.

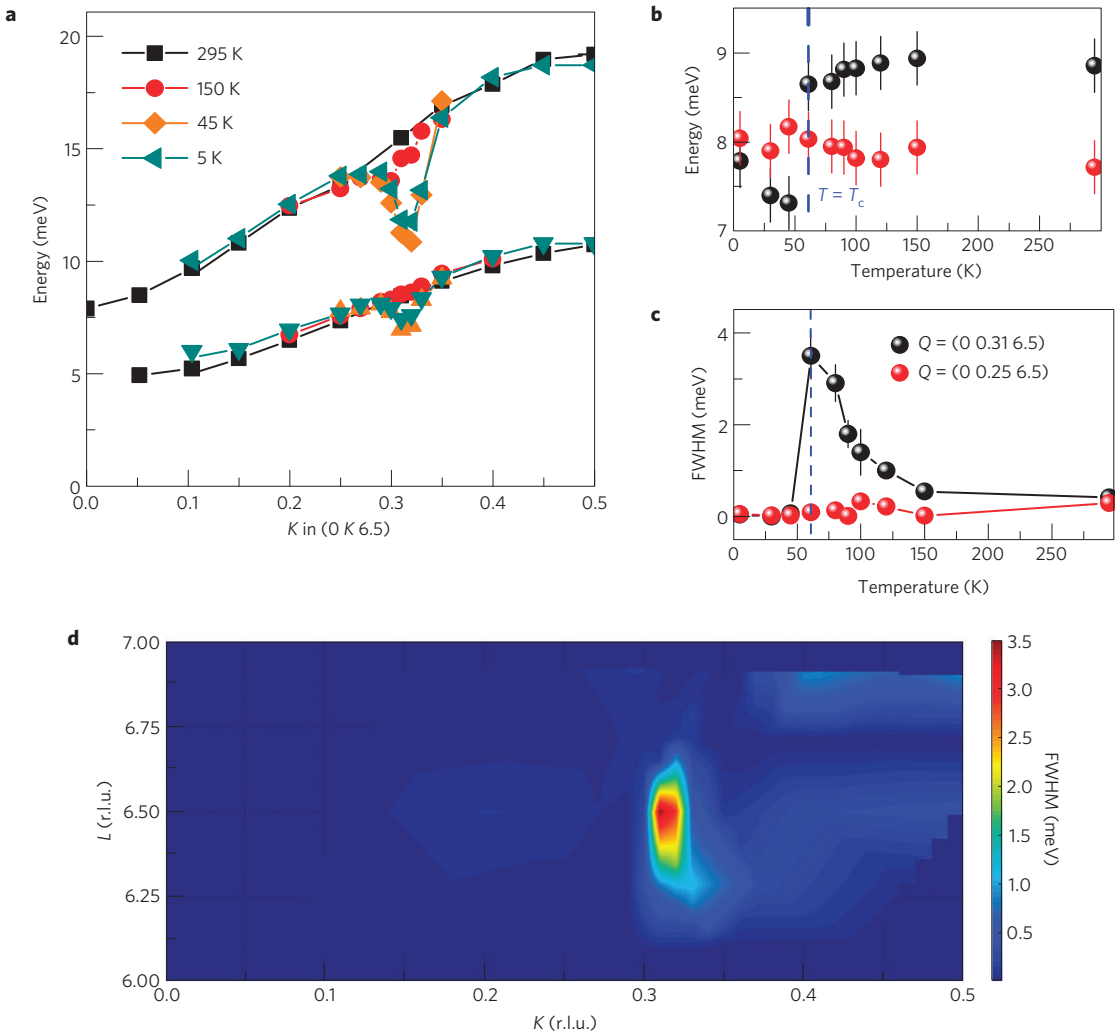

Figure 4 | Temperature dependence of the phonon dispersion. a, Dispersion of the two low-energy phonons in the Z–T direction at $T = 295$, 150, 45 and 5 K. **b**,**c**, Temperature dependence of the acoustical phonon energy and FWHM, respectively, at $\mathbf{Q} = (0\ 0.25\ 6.5)$ (red dots) and $\mathbf{Q} = (0\ 0.31\ 6.5)$ (black dots). In both panels, error bars represent the fit uncertainty. **d**, Momentum dependence of the intrinsic FWHM of the transverse acoustic phonon at $T = T_c$.

The momentum and temperature dependence of the elastic intensity in the IXS spectra of $YBa_2Cu_3O_{6.6}$ is reminiscent of the behaviour of other materials undergoing structural phase transitions, including insulating $SrTiO_3$ (ref. 20), superconducting Nb_3Sn (ref. 21) and metallic $ZrTe_3$ (ref. 23). In these compounds, an elastic 'central peak' appears in the fluctuation regime above the critical temperature, where it is understood as defect-induced nucleation of finite-size domains of the low-temperature phase. The nature of the lattice defects responsible for the central peak in these materials has remained undetermined, although oxygen vacancies were shown to play some role in $SrTiO_3$ (ref. 20). In $YBa_2Cu_3O_{6+x}$, both local lattice distortions generated by oxygen defects in the CuO chains and extended defects such as dislocations may act as pinning centres for CDW nanodomains. The extremely large phonon linewidths in the normal state (Fig. 4c,d) can then be attributed to inhomogeneous broadening.

As doping-induced lattice defects are present in all superconducting cuprates, the gradual onset of a spatially inhomogeneous CDW domain state with decreasing temperature may be a generic feature of the 'pseudogap' regime in the cuprate phase diagram, although the temperature and doping dependence of the corresponding volume fractions may depend on the specific realization of lattice disorder in different materials. Whereas CDW nanodomains will surely contribute to the anomalous normal-state properties observed in this regime, their gradual nucleation explains the absence of thermodynamic singularities associated with CDW order, at least in the absence of a magnetic field[40]. The persistence of this domain state over a much wider temperature range than corresponding phenomena in classical materials[20,21] probably reflects the strong competition between CDW correlations and superconductivity. In the presence of superconducting long-range order, the inhomogeneity is strongly reduced (Figs 4 and 5). Conversely, thermodynamic singularities[40] and NMR signals[41,42] due to CDW long-range order have been reported in external magnetic fields strong enough to weaken or obliterate superconductivity. The fragility of the CDW nanodomain state in zero field and its competition with superconductivity explain the isotope effect on the superconducting penetration depth observed in the $YBa_2Cu_3O_{6+x}$ system[43]. We also note the close analogy of our observations to the 'charge glass' state previously identified by STS at low doping levels[32], and to the nucleation of antiferromagnetic domains by spinless impurities studied by NMR (ref. 44) and neutron scattering[45].

We end our discussion with some remarks about the implications of our results for the mechanism of high-temperature superconductivity. As it involves low-energy phonons, the large superconductivity-induced renormalization revealed by our IXS study probably accounts for a large part of the total electron–phonon coupling. It seems strong enough to be a major contributor

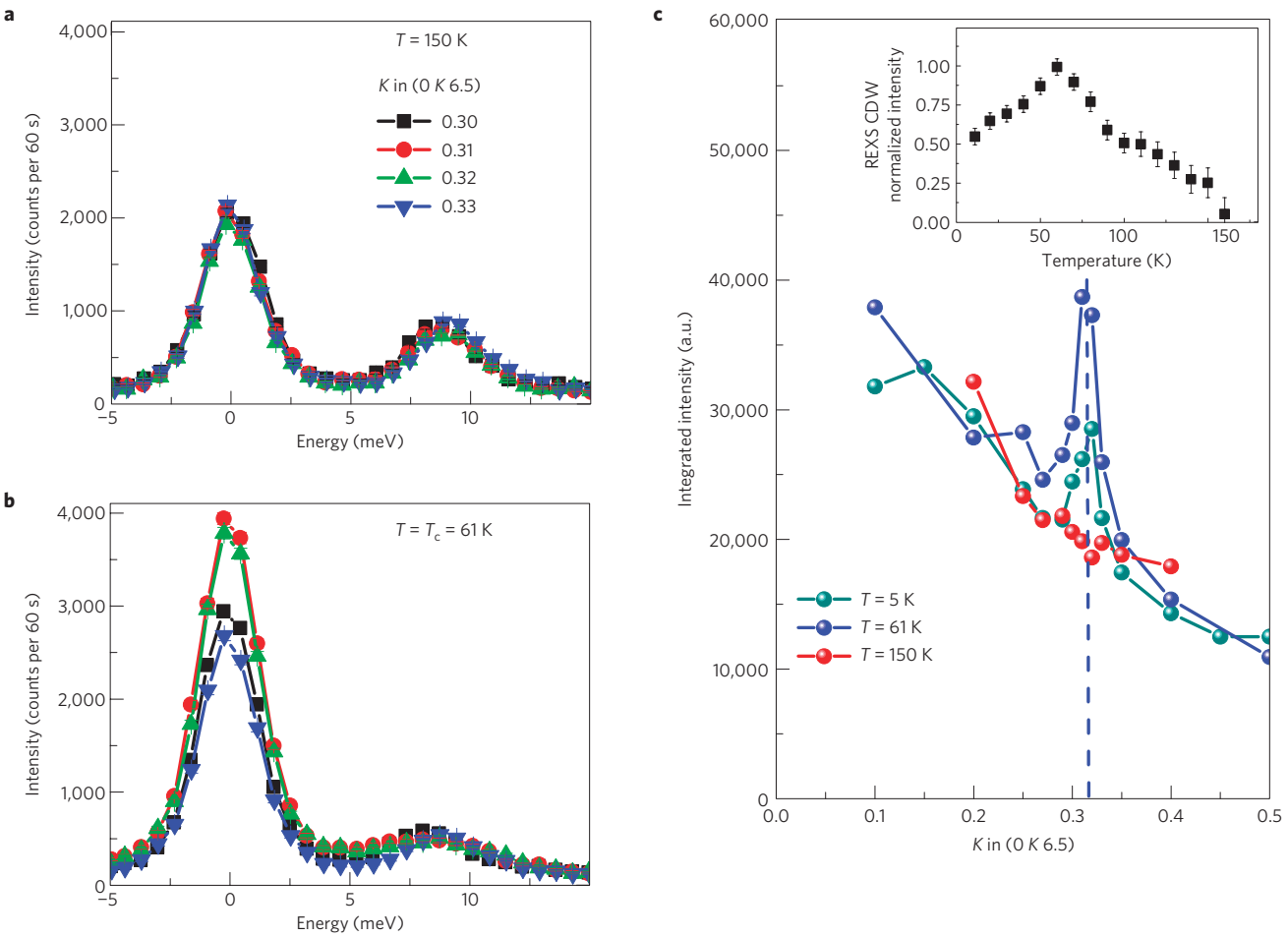

Figure 5 | Temperature dependence of the central peak. a,**b**, IXS spectra in the vicinity of $\mathbf{q}_{CDW}$ at $T = 150$ K and $T = T_c = 61$ K, respectively, normalized for the Bose thermal excitation factor. Error bars represent the statistical error. **c**, Momentum dependence of the intensity of the central peak at $T = 150$, 90, 61 and 5 K. The inset shows the temperature dependence of the CDW peak seen with resonant X-ray scattering[15].

to at least some of the 'kinks' observed in the dispersions of fermionic quasiparticles in the cuprates. As it is very sharply concentrated in momentum space, however, its momentum-averaged strength seems insufficient to be a significant driving force for Cooper pair formation. Rather, the EPI favours a CDW instability that strongly competes with superconductivity and reduces the superconducting T_c at moderate doping levels. We have confirmed these conclusions by repeating some of the IXS experiments on a fully oxygenated $YBa_2Cu_3O_7$ crystal with $T_c = 90$ K (Supplementary Information), where we found neither phonon anomalies characteristic of incipient CDW formation nor a central peak heralding CDW nanodomains.

Note added in proof. During the review process of this Article, we became aware of work on ortho-II $YBa_2Cu_3O_{6.54}$ in which similar temperature dependence of the elastic line and broadening of the low-energy phonon are reported above the superconducting transition[46].

Received 17 July 2013; accepted 11 October 2013; published online 24 November 2013

References

1. Gunnarsson, O. & Rösch, O. Interplay between electron–phonon and Coulomb interactions in cuprates. *J. Phys. Condens. Matter* **20,** 043201 (2008).
2. Capone, M., Castellani, C. & Grilli, M. Electron–phonon interaction in strongly correlated systems. *Adv. Condens. Matter Phys.* **2010,** 920860 (2010).
3. Reznik, D. Phonon anomalies and dynamic stripes. *Physica C* **481,** 75–92 (2012).
4. Savrasov, S. Y. & Andersen, O. K. Linear-response calculation of the electron–phonon coupling in doped $CaCuO_2$. *Phys. Rev. Lett.* **77,** 4430–4433 (1996).
5. Bohnen, K-P., Heid, R. & Krauss, M. Phonon dispersion and electron–phonon interaction for $YBa_2Cu_3O_7$ from first-principles calculations. *Europhys. Lett.* **64,** 104–110 (2003).
6. Giustino, F., Cohen, M. L. & Louie, S. G. Small phonon contribution to the photoemission kink in the copper oxide superconductors. *Nature* **452,** 975–978 (2008).
7. Heid, R., Zeyher, R., Manske, D. & Bohnen, K-P. Phonon-induced pairing interaction in $YBa_2Cu_3O_7$ within the local-density approximation. *Phys. Rev. B* **80,** 024507 (2009).
8. Cuk, T. *et al.* Coupling of the B_{1g} phonon to the antinodal electronic states of $Bi_2Sr_2Ca_{0.92}Y_{0.08}Cu_2O_{8+\delta}$. *Phys. Rev. Lett.* **93,** 117003 (2004).
9. Devereaux, T. P., Cuk, T., Shen, Z. X. & Nagaosa, N. Anisotropic electron–phonon interaction in the cuprates. *Phys. Rev. Lett.* **93,** 117004 (2004).
10. Vishik, I. M. *et al.* Doping-dependent nodal Fermi velocity of the high-temperature superconductor $Bi_2Sr_2CaCu_2O_{8+}$ delta revealed using high-resolution angle-resolved photoemission spectroscopy. *Phys. Rev. Lett.* **104,** 207002 (2010).
11. Johnston, S. *et al.* Evidence for the importance of extended Coulomb interactions and forward scattering in cuprate superconductors. *Phys. Rev. Lett.* **108,** 166404 (2012).
12. Pintschovius, L. *et al.* Pronounced in-plane anisotropy of phonon anomalies in $YBa_2Cu_3O_{6.6}$. *Phys. Rev. Lett.* **89,** 037001 (2002).
13. Reznik, D. *et al.* Electron–phonon coupling reflecting dynamic charge inhomogeneity in copper oxide superconductors. *Nature* **440,** 1170–1173 (2006).

14. Raichle, M. *et al.* Highly anisotropic anomaly in the dispersion of the copper–oxygen bond-bending phonon in superconducting $YBa_2Cu_3O_7$ from inelastic neutron scattering. *Phys. Rev. Lett.* **107,** 177004 (2011).
15. Ghiringhelli, G. *et al.* Long-range incommensurate charge fluctuations in $(Y,Nd)Ba_2Cu_3O_{6+x}$. *Science* **337,** 821–825 (2012).
16. Chang, J. *et al.* Direct observation of competition between superconductivity and charge density wave order in $YBa_2Cu_3O_{6.67}$. *Nature Phys.* **8,** 871–876 (2012).
17. Achkar, A. J. *et al.* Distinct charge orders in the planes and chains of ortho-III-ordered $YBa_2Cu_3O_{6+\delta}$ superconductors identified by resonant elastic x-ray scattering. *Phys. Rev. Lett.* **109,** 167001 (2012).
18. Blackburn, E. *et al.* X-ray diffraction observations of a charge-density-wave order in superconducting ortho-II $YBa_2Cu_3O_{6.54}$ single crystals in zero magnetic field. *Phys. Rev. Lett.* **110,** 137004 (2013).
19. Blanco-Canosa, S. *et al.* Momentum-dependent charge correlations in $YBa_2Cu_3O_{6+\delta}$ superconductors probed by resonant X-Ray scattering: Evidence for three competing phases. *Phys. Rev. Lett.* **110,** 187001 (2013).
20. Cowley, R. J. The phase transition of strontium titanate. *Phil. Trans. R. Soc. Lond. A* **354,** 2799–2814 (1996).
21. Axe, J. D. & Shirane, G. Inelastic-neutron-scattering study of acoustic phonons in Nb_3Sn. *Phys. Rev. B* **8,** 1965–1977 (1973).
22. Leroux, M. *et al.* Anharmonic suppression of charge density waves in 2H-NbS_2. *Phys. Rev. B* **86,** 155125 (2012).
23. Hoesch, M. *et al.* Giant Kohn anomaly and the phase transition in charge density wave $ZrTe_3$. *Phys. Rev. Lett.* **102,** 086402 (2009).
24. Andersen, N. H. *et al.* Superstructure formation and the structural phase diagram of $YBa_2Cu_3O_{6+x}$. *Physica C* **317,** 259–269 (1999).
25. Strempfer, J. *et al.* Oxygen superstructures throughout the phase diagram of $(Y,Ca)Ba_2Cu_3O_{6+x}$. *Phys. Rev. Lett.* **93,** 157007 (2004).
26. Bonnoit, C. J. *et al.* Probing electronic order via coupling to low energy phonons in superconducting $Bi_2Sr_{2-x}La_xCuO_{6+\delta}$. Preprint at http://arxiv.org/abs/1202.4994 (2012).
27. Renker, B. *et al.* Observation of giant Kohn anomaly in the one-dimensional conductor $K_2Pt(CN)_4Br_{0.3}\cdot 3H_2O$. *Phys. Rev. Lett.* **30,** 1144–1147 (1973).
28. Weber, F. *et al.* Extended phonon collapse and the origin of the charge-density wave in 2H-$NbSe_2$. *Phys. Rev. Lett.* **107,** 107403 (2011).
29. Castellani, C., Di Castro, C. & Grilli, M. Singular quasiparticle scattering in the proximity of charge instabilities. *Phys. Rev. Lett.* **75,** 4650–4653 (1995).
30. McElroy, K. *et al.* Relating atomic scale electronic phenomena to wave-like quasiparticle states in supercondconducting $Bi_2Sr_2CaCu_2O_{8+\delta}$. *Nature* **422,** 592–596 (2003).
31. Howald, C., Eisaki, H., Kaneko, N., Greven, M. & Kapitulnik, A. Periodic density-of-states modulations in superconducting $Bi_2Sr_2CaCu_2O_{8+\delta}$. *Phys. Rev. B* **67,** 014533 (2003).
32. Kohsaka, Y. *et al.* An intrinsic bond-centered electronic glass with unidirectional domains in underdoped cuprates. *Science* **315,** 1380–1385 (2007).
33. Wise, W. D. *et al.* Charge-density-wave origin of cuprate checkerboard visualized by scanning tunnelling microscopy. *Nature Phys.* **4,** 696–699 (2008).
34. Parker, C. V. *et al.* Fluctuating stripes at the onset of the pseudogap in the high-T_c superconductor $Bi_2Sr_2CaCu_2O_{8+x}$. *Nature* **468,** 677–680 (2010).
35. Hinton, J. P. *et al.* New collective mode in $YBa_2Cu_3O_{6+x}$ observed by time-domain reflectometry. *Phys. Rev. B* **88,** 060508 (2013).
36. Torchinsky, D. H. *et al.* Fluctuating charge-density waves in a cuprate superconductor. *Nature Mater.* **12,** 387–391 (2013).
37. Aynajian, P. *et al.* Energy gaps and Kohn anomalies in elemental superconductors. *Science* **319,** 1509–1512 (2008).
38. Friedl, B., Thomsen, C. & Cardona, M. Determination of the superconducting gap in $RBa_2Cu_3O_{7-\delta}$. *Phys. Rev. Lett.* **65,** 915–918 (1990).
39. Bakr, M. *et al.* Electronic and phononic Raman scattering in detwinned $YBa_2Cu_3O_{6.95}$ and $Y_{0.85}Ca_{0.15}Ba_2Cu_3O_{6.95}$: *s*-wave admixture to the $d_{x^2-y^2}$-wave order parameter. *Phys. Rev. B* **80,** 064505 (2009).
40. LeBoeuf, D. *et al.* Thermodynamic phase diagram of static charge order in underdoped $YBa_2Cu_3O_y$. *Nature Phys.* **9,** 79–83 (2013).
41. Wu, T. *et al.* Magnetic-field-induced charge-stripe order in the high-temperature superconductor $YBa_2Cu_3O_y$. *Nature* **477,** 191–194 (2011).
42. Wu, T. *et al.* Emergence of charge order from the vortex state of a high-temperature superconductor. *Nature Commun.* **4,** 2113 (2013).
43. Khasanov, R. *et al.* Oxygen isotope effects on the superconducting transition and magnetic states within the phase diagram of $Y_{1-x}Pr_xBa_2Cu_3O_{7-\delta}$. *Phys. Rev. Lett.* **101,** 077001 (2008).
44. Alloul, H., Bobroff, J., Gabay, M. & Hirschfeld, P. J. Defects in correlated metals and superconductors. *Rev. Mod. Phys.* **81,** 45–108 (2009).
45. Suchaneck, A. *et al.* Incommensurate magnetic order and dynamics induced by spinless impurities in $YBa_2Cu_3O_{6.6}$. *Phys. Rev. Lett.* **105,** 037207 (2010).
46. Blackburn, E. *et al.* Inelastic x-ray study of phonon broadening and charge-density wave formation in ortho-II-ordered $YBa_2Cu_3O_{6.54}$. *Phys. Rev. B* **88,** 054506 (2013).

Acknowledgements

This work was performed at the ID28 (IXS) and ID29 (DS) beamlines of the European Synchrotron Radiation Facility. We gratefully acknowledge L. Braicovich, M. Calandra, R. Comin, A. Damascelli, T. Devereaux, M. H. Julien, A. F. Kemper, G. Khaliullin, O. Gunnarsson, G. A. Sawatzky and R. Zeyher for insightful discussions.

Author contributions

M.L.T., G.G. and B.K. managed the project. T.L. prepared and characterized the single crystal. A.B. performed the diffuse scattering experiment. M.L.T., A.B., S.M.S. and G.D. carried out the IXS experiment. M.L.T., S.M.S. and G.D. analysed the data. R.H. and K-P.B. performed calculations. M.L.T. and B.K. wrote the paper with helpful comments from all co-authors.

Additional information

Supplementary information is available in the online version of the paper. Reprints and permissions information is available online at www.nature.com/reprints. Correspondence and requests for materials should be addressed to M.L.T. or B.K.

Competing financial interests

The authors declare no competing financial interests.